First observation of excited states in the $T_z=1/2$ nucleus ^{85}Mo

N. Mărginean,[1,2] C. Rossi Alvarez,[3] D. Bucurescu,[2] Yang Sun,[4,5] C. A. Ur,[3,2] A. Gadea,[1] S. Lunardi,[3] D. Bazzacco,[3] G. de Angelis,[1] M. Axiotis,[1] M. De Poli,[1] E. Farnea,[1,3] M. Ionescu–Bujor,[2] A. Iordăchescu,[2] S. M. Lenzi,[3] Th. Kröll,[1,3] T. Martinez,[1] R. Menegazzo,[3] D. R. Napoli,[1] G. Nardelli,[7] P. Pavan,[3] B. Quintana,[3,8] and P. Spolaore[1]

[1]*INFN, Laboratori Nazionali di Legnaro, Italy*

[2]*H.Hulubei National Institute for Physics and Nuclear Engineering, Bucharest, Romania*

[3]*Dipartimento di Fisica dell'Università and INFN, Sezione di Padova, Italy*

[4]*Department of Physics and Astronomy, University of Tennessee, Knoxville, Tennessee 37996*

[5]*Department of Physics, Xuzhou Normal University, Xuzhou, Jiangsu 221009, People's Republic of China*

[6]*Instituto de Física Corpuscular, Valencia, Spain*

[7]*Dipartimento di Chimica Fisica dell'Università di Venezia and INFN, Sezione di Padova, Italy*

[8]*Grupo de Física Nuclear, Universidad de Salamanca, Spain*

(Received 29 May 2001; published 1 March 2002)

Excited states in the $T_z=\frac{1}{2}$ nucleus ^{85}Mo have been observed for the first time with the reaction ^{58}Ni(^{32}S, $\alpha n\gamma$) at 105 MeV. γ-ray transitions in this nucleus have been assigned unambiguously by combining the information from the GASP γ-ray array, the ISIS silicon ball, and the *n*-Ring neutron detector. Two band structures have been observed in this nucleus; they continue the smooth evolution of the known bands from the lighter $N=43$ isotones and have been tentatively assigned spins and parity on this basis. After reaching a maximum of collectivity at ^{83}Zr, the trend with increasing mass is reversed, showing a smaller collectivity at ^{85}Mo. The rotational behavior of the observed bands is discussed on the basis of the projected shell model calculations.

DOI: 10.1103/PhysRevC.65.034315 PACS number(s): 21.10.Re, 23.20.Lv, 25.70.Jj, 27.50.+e

I. INTRODUCTION

The nuclei in the immediate vicinity of the $N=Z$ line and with mass above 80 constitute one of the regions of current interest, and there have been continuous efforts to study their structure in a systematic manner. Being close to the proton drip line, this region is hardly accessible with the available (stable) target-projectile combinations. Indeed, on the $N=Z$ line, which is the most difficult to study, the progress during the past years was extremely slow, the heaviest nucleus in which a few excited states could be recently determined being the even-even nucleus ^{88}Ru [1]. The $N=Z+1$ line ($T_z=1/2$ nuclei) has been mapped for all masses up to 83, and some information (a cascade of two γ-ray transitions) has been obtained in ^{87}Tc [2], while nothing is known on the excited levels of the ^{85}Mo nucleus. The only experimental information about this nucleus is obtained from a β-delayed proton decay study, and concerns the ground state which is assigned as $J^\pi=1/2^-$ [3].

One of the points of interest in the study of the $A>80$ nuclei on and near the $N=Z$ line is the fact that they cover a transitional region with a fast evolution [1,4] from nuclei with the largest known ground state deformation (centered on ^{76}Sr [5] and ^{80}Zr [6]), towards the (probably spherical) doubly magic ^{100}Sn. The study of the odd-mass nuclei in this region may provide experimental probes of the neighboring even-even transitional nuclei. Another reason for studying this remote nuclear region is the hope to observe effects of the collective neutron-proton (np) pairing interaction. Effects of this interaction are expected to be strongest in the $N=Z$ nuclei (which have the largest relative number of np pairs) and it is a topical subject how to recognize them. They may be also enhanced in their closest neighbors, the nuclei along the $N=Z+1$ line, although until now the understanding of the observed characteristics did not seem to require an explicit consideration of this interaction in conventional total routhian surface calculations [7]. Nevertheless, it is important to have a more complete image, as systematic as possible, of the evolution of the nuclear structure of the $N=Z+1$ nuclei from this mass region, such as to allow more global assessments of the theoretical model analyses.

The purpose of this article is to present the first experimental observation of excited states in ^{85}Mo. These results are then compared with calculations performed with the projected shell model.

II. EXPERIMENT

The ^{85}Mo nucleus was populated in the reaction ^{58}Ni $+^{32}$S at an incident energy of 105 MeV. The $^{32}S^{8+}$ beam, with an intensity of about 6 particle nA was delivered by the Legnaro XTU Tandem accelerator. The target consisted of a 1.1 mg/cm^2 ^{58}Ni layer evaporated on a 10 mg/cm^2 Au foil. The incident beam energy was chosen such as to favor the two particle evaporation channels.

The γ rays were detected with the GASP array [8] in its standard configuration with 40 Compton-suppressed HPGe detectors and a BGO inner ball. Six elements, out of the 80 of the inner ball, placed on the most forward ring were replaced with the *n*-Ring detector [9]. The *n*-Ring consists of six BC501A liquid scintillator filled detectors for neutron-γ discrimination. The ISIS silicon ball [10], consisting of 40 ΔE-E telescopes with a geometry similar to that of GASP, was also used. The trigger condition required at least 2 Ge and 3 BGO detectors firing in coincidence. A total number of

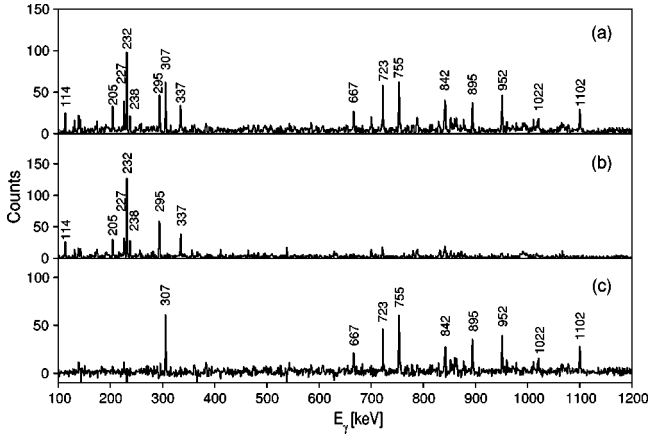

FIG. 1. (a) Projection of a γ-γ coincidence matrix obtained in coincidence with one α particle, ''zero'' protons (i.e., anticoincidence with protons detected in ISIS), and neutrons; the γ-ray peaks are transitions in ^{84}Nb and ^{85}Mo. (b) Same as above, but for a γ-γ matrix coincident with one α particle, one proton, and neutrons; the spectrum contains only transitions from ^{84}Nb (Ref. [11]). (c) Difference between the upper two spectra, normalized according to the measured proton detection efficiency. The γ lines left belong to the αn channel (the ^{85}Mo nucleus, see text).

10^9 events have been recorded in a 6 day experiment.

In the off-line processing of the data, a clean neutron identification was achieved by setting two selection conditions, one on the time of flight-zero crossover (ZCO) time distribution, and the other on the energy-ZCO distribution. In this way, the γ rays coming from nuclei formed without evaporation of neutrons were reduced by a factor of more than 10^4 when the coincidence with neutrons was requested. The experimental values of the particle detection efficiencies were $\sim$56% for detecting one proton, 36% for one α particle, and 3.1% for one neutron.

The information on the charged particles, deduced from the ISIS data, consists of the type and multiplicity of the detected particles. γ-γ coincidence matrices have been sorted with different conditions concerning the detected charged particles and neutrons and used to assign the γ rays due to the prompt decay of excited states of ^{85}Mo as described below.

III. RESULTS

Figure 1 illustrates the procedure of assigning γ rays to the prompt decay of ^{85}Mo levels. The upper part shows the projection of a γ-γ coincidence matrix which we shall call ''$1\alpha 0pn$;'' this matrix has been obtained by requiring coincidence with one α-particle, ''zero'' protons (that is, by accepting the sorted event only if ISIS did not detect any proton), and neutrons (in any number). The zero proton condition has been set in order to reduce as much as possible the background due to the proton-evaporation channels. Note that, however, due to the proton detection efficiency less than 100% the channel $1\alpha 1p1n$ (^{84}Nb [11]) still appears in this matrix. On the other hand, the excellent neutron-γ discrimination completely suppressed the very strong channels $1\alpha 1p$ (^{85}Nb) and $1\alpha 2p$ (^{84}Zr).

TABLE I. Relative intensities of the γ-ray transitions assigned to ^{85}Mo (see Fig. 2 for their placement into the level scheme).

E_γ (keV)	I_γ	E_γ (keV)	I_γ
306.7	66(7)	865.0	12(5)
360.5	11(4)	879.1	37(4)
362.9	11(3)	895.5	51(5)
384.8	18(4)	952.3	85(8)
667.2	34(6)	1012.9	23(8)
723.4	69(8)	1021.9	35(6)
754.8	100(9)	1069.2	16(3)
790.6	22(6)	1079.4	19(4)
842.4	44(5)	1101.8	75(8)
861.6	27(8)		

The middle part of Fig. 1 shows the projection of the $1\alpha 1pn$ γ-γ coincidence matrix (obtained in coincidence with one α particle, one proton, and neutrons). This matrix contains practically only the $1\alpha 1p1n$ channel (^{84}Nb) [11].

A comparison of the two spectra discussed above readily shows the γ rays which are in coincidence with one α-particle *and* with neutrons, but *not* in coincidence with protons, and therefore must be assigned to a Mo isotope. These are shown in the lowest pannel of Fig. 1, which shows the spectrum resulted from the difference of the upper two spectra, normalized according to the measured proton detection efficiency. Since the two known yrast γ rays of ^{84}Mo (channel $1\alpha 2n$), of 444 and 674 keV [4], are not seen, it is clear that all the γ rays observed in this way can be unambiguously assigned to the $1\alpha 1n$ channel, i.e., ^{85}Mo.

First coincidence relationships between the ^{85}Mo γ rays have been obtained from the $1\alpha 0pn$ matrix, but, once the main γ rays of ^{85}Mo have been recognized, the level scheme could be constructed by working on the $1\alpha 0p$ matrix, in which the αn chanel had much better statistic. The level scheme built on the basis of coincidence relationships and relative intensities (given in Table I) is shown in Fig. 2. Two sets of levels (band structures), which could not be interconnected by any transition, have been observed. Their assignment will be discussed below. The two band structures are illustrated by gated γ-ray spectra in Fig. 3.

The intensities of all reaction channels sizably populated in our reaction have been deduced from the coincidence spectra of the two lowest transitions of the structures populated in each nucleus and corrected for efficiency (usually, for the odd-A and odd-odd nuclei there are more such structures, so finally one sums their intensities); the sum of all channels was then normalized to the fusion cross section calculated with the code CASCADE for an incident energy of 100 MeV (the beam energy at the middle of the target). In this way, we estimate that the αn channel was populated with a cross section of about 0.13 mb.

A tentative assignment of spins and parities of the observed levels could be made on the basis of the examination of the systematic behavior of the band structures known in the $N=43$ isotones. Figure 4 shows that the two band structures assigned to ^{85}Mo (the heaviest studied $N=43$ nucleus)

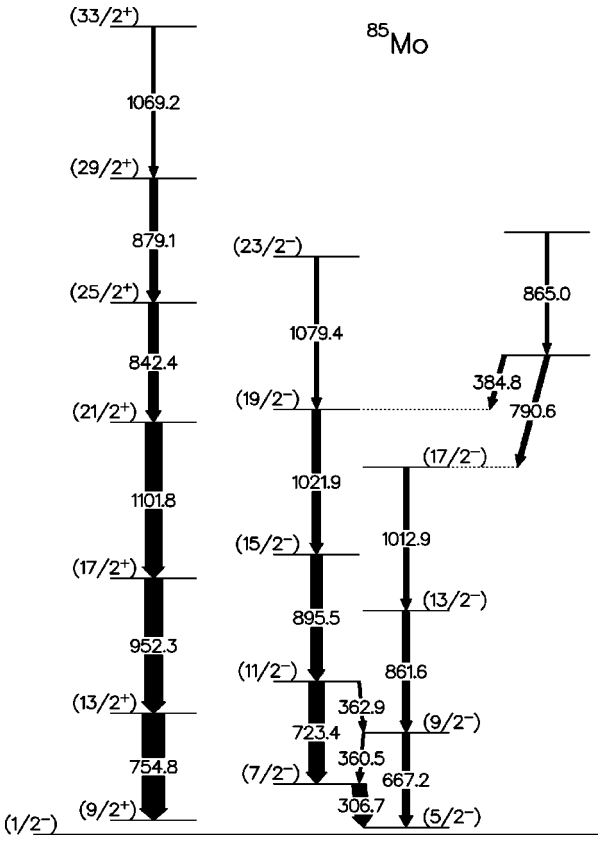

FIG. 2. The level scheme of ^{85}Mo, as observed in the present experiment. The tentative spin and parity assignments are made on the basis of experimental systematics (see discussion in Sec. III). The excitation energies of the $(5/2)^-$ and $(9/2)^+$ bandheads is undetermined, but we place them tentatively at 30 and 150 keV, respectively, according to the $N=43$ systematic (Fig. 5 and text).

continue rather smoothly the evolution of two band structures systematically observed in the lighter isotones. The sequence most strongly populated in our nucleus (starting with the 755 keV transition) is very similar to the $\alpha=+1/2$ signature of the rotation-aligned positive-parity band due to the

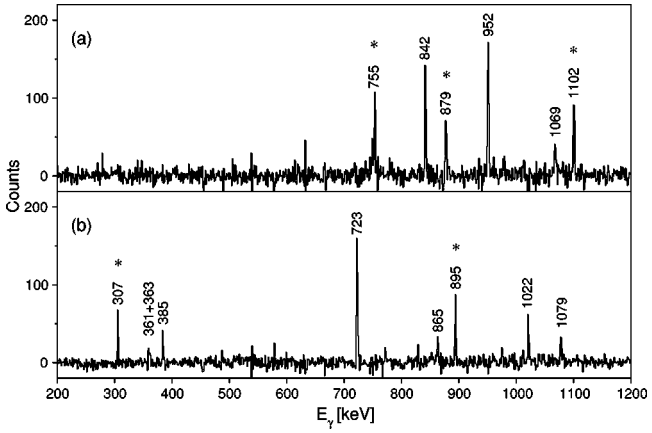

FIG. 3. Gated γ-ray spectra showing the band structures of Fig. 2. The γ-ray gates were set on ''clean'' transitions (i.e., belonging only to ^{85}Mo), as indicated by an asterisk, in the $1\alpha 0p$ γ-γ (see text) coincidence matrix.

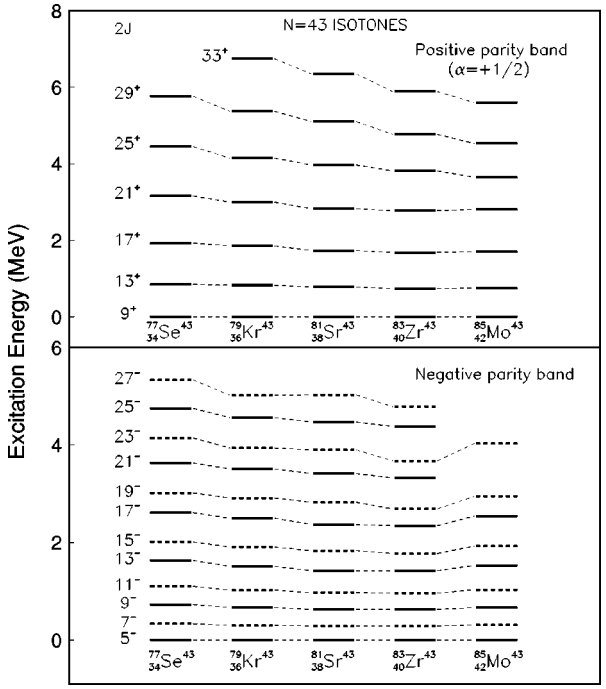

FIG. 4. Systematic of band structures in the $N=43$ isotones. The experimental information is as folows: ^{77}Se: [14]; ^{79}Kr: [14]; ^{81}Sr: [16,17]; ^{83}Zr: [18,19]; ^{85}Mo: present data.

$g_{9/2}$ orbital and based on a $9/2^+$ state [12–18]. We were not able to observe members of the other signature ($\alpha=-1/2$) of this structure. The other sequence, with two bands interconnected in the lowest part, continues smoothly the evolution of a strongly coupled band of negative parity built on a $5/2^-$ state [12–18]. Due to this remarkable similarity we have tentatively assigned spins and parities to the two band structures as shown in Fig. 2. Another band observed in the lighter isotones ^{77}Se [12] and ^{79}Kr [14] is the one built on the $1/2^-$ ground state. Since the lowest transitions in this band have lower energies (the $5/2^-\rightarrow 1/2^-$ transition is 439 and 402 keV, respectively, in the above nuclei), which do not fit with the values in our bands, it is unlikely that any of the bands observed in this experiment is built on the $1/2^-$ ground state.

In the region above the $(17/2^-)$ and $(19/2^-)$ states we found some levels connected only to the negative-parity bands (the levels drawn to the right of the negative parity band in Fig. 2). Such side structures have also been observed in the other $N=43$ isotones: ^{77}Se [12], ^{79}Kr [13], and ^{83}Zr [18].

Indications about the multipolarities of the transitions, which support these assignments, could be obtained only for the two strongest lower transitions, of 754.8 and 306.7 keV, respectively. For these transitions, we have determined the angular distribution from oriented states (ADO) ratio, defined as the ratio between the average intensity of the transition in the detector rings at 36° and 144°, and that in the 90° detector ring, in $1\alpha 0p$ matrices. This ratio should be about 1.2 for a pure stretched $E2$ transition and about 0.7 for a pure $M1$ stretched transition. The values we have obtained are 1.12(18) for the 755 keV transition and 1.21(20) for the

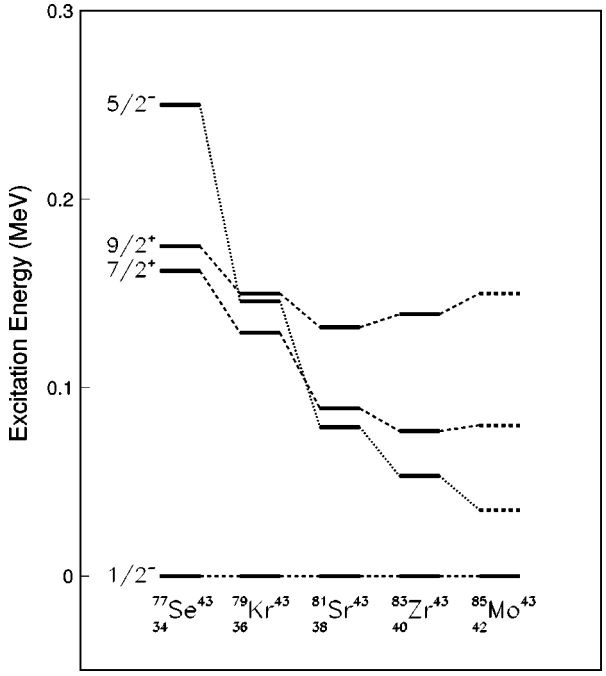

FIG. 5. Systematic of the lowest energy levels in the $N=43$ isotones (Refs. [14–19]). A smooth extrapolation is suggested for ^{85}Mo.

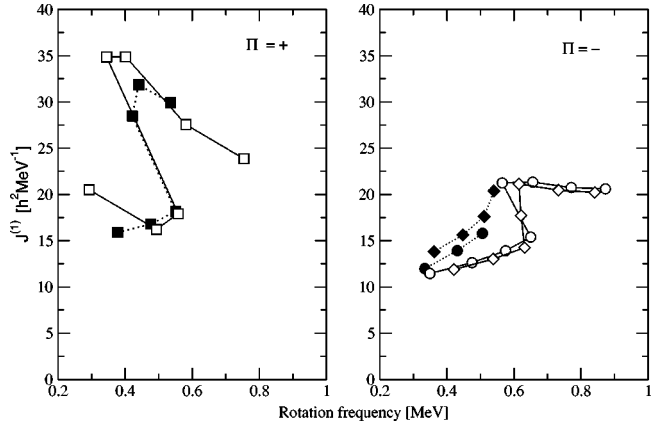

FIG. 6. The kinematic moments of inertia in the two band structures observed in ^{85}Mo, compared to results of projected shell model calculations. The full symbols represent experimental data, the empty ones the calculations.

307 keV transition. These values, together with the pattern of the constructed level scheme (Fig. 2) and the systematic of the band structures in this mass region (Fig. 3), are compatible with a quadrupole character of the 755 keV line, and a mixed dipole/quadrupole character of the 307 keV line; indeed, in some other $N=43$ isotones, the $7/2^- \rightarrow 5/2^-$ transition is found compatible with a dipole ($M1$) mixed with a large quadrupole ($E2$) component [12,13,15,17]. For other transitions we could not determine these values, since practically all of them are made impure with much stronger γ rays from other channels (e.g., 723 keV, with a line of ^{84}Zr [20], the $\alpha 2p$ channel; 667 keV with a line in ^{85}Nb [19], the αp channel, etc.).

Another problem concerns the relative position of the two band structures with respect to the ground state. A hint may be obtained by following the evolution of the excitation energies of the lowest excited states in the lighter isotones, which is shown in Fig. 5. The ground state is a $J^\pi = 1/2^-$ in all these nuclei up to ^{83}Zr, and the β-delayed proton emission study of Ref. [3] supports a similar assignment for the ground state of ^{85}Mo. A smooth extrapolation of the excitation energy of the lowest $5/2^-$, $7/2^+$ (bandheads) and $9/2^+$ states leads to the following suggestions for ^{85}Mo. The $5/2^-$ state, which is rather low (below 100 keV) in both ^{81}Sr and ^{83}Zr shows a steadily decreasing energy, and consequently one may expect that it is still lower in ^{85}Mo, around 30–40 keV. It is likely that we were not able to observe the transition from this state to the $1/2^-$ ground state due to its low energy. According to the trend shown in the same figure, one might expect the $7/2^+$ state to be around 70 keV, about the same as in ^{83}Zr [17]. In both ^{81}Sr [15,16] and ^{83}Zr [17,18] this state is known to decay to the $5/2^-$ state by a very small energy transition (10 and 24 keV, respectively); for ^{85}Mo, the systematic of Fig. 5 indicates a possible increase (to 40–50 keV) of the separation energy between the two states, too small, however, to have been observed in our experiment, in which the effective threshold was around 60 keV. The $9/2^+$ state in ^{85}Mo is expected at an excitation energy around 150 keV, above the $7/2^+$ state. We have not observed, however, the expected transition between these states. One should emphasize once more that the placement of the two band structures with respect to the $1/2^-$ ground state, as shown in Fig. 2, is only tentative based on the isotonic systematic of Fig. 5.

IV. GENERAL DISCUSSION

The systematic evolution of the two band structures considered above, for the $N=43$ isotones between Se and Zr, was extensively discussed in previous papers [12,13]. Also, for all these nuclei [12–18], the properties of these band structures were interpreted in the framework of the deformed Woods-Saxon cranking model [22]. In the following we shall consider an extension of these systematics and discussion to ^{85}Mo. From Fig. 4 one observes that the two rotational band structures reach a maximum of collectivity at ^{83}Zr and become somewhat less collective (higher transition energies) in ^{85}Mo.

Figure 6 displays the variation of the kinematic moment of inertia of the two bands. The left side shows the positive-parity band, for which we observed only the $9/2^+$, $13/2^+$, $17/2^+$, ... sequence (with signature $\alpha = +1/2$). In the other nuclei the $\alpha = -1/2$ signature partner is also known [12–18], but it was observed with much lower intensity, which would explain why it was difficult to see it in the present case. The $\alpha = +1/2$ band presents systematic changes, from an upbending in ^{77}Se and ^{79}Kr, to a sharp backbending in ^{83}Zr (see, e.g., Ref. [12]). ^{85}Mo continues this trend, showing an even sharper backbending. Since the $\nu g_{9/2}$ orbital is blocked, this irregularity has been interpreted as the alignment of a $g_{9/2}$ proton pair. The crossing between the 1qp ($\nu g_{9/2}$) and 3qp ($\nu g_{9/2} \otimes \pi g_{9/2}^2$) configurations takes place at a rotational

frequency $\hbar\omega \simeq 0.50$ MeV in ^{85}Mo, very similar with that in ^{83}Zr. This rotational frequency is also comparable to that of the first backbending in the g.s.b. of the even-even core nucleus ^{86}Mo, which occurs at $\hbar\omega = 0.48$ MeV and has also been interpreted as due to the $g_{9/2}$ proton alignment [21].

Figure 6 shows also the behavior of both signatures of the negative-parity band. ^{85}Mo continues smoothly the evolution observed in its isotones with increasing Z [12], showing the beginning of an upbending (in the $\alpha = -1/2$ signature member) at the same frequency, of ≈ 0.50 MeV, which has also been interpreted as the alignment of a $g_{9/2}$ proton pair.

The positive-parity sequence was interpreted in all the other $N = 43$ isotones as a rotation-aligned band based on the [422]5/2 Nilsson orbital. In the lighter $N = 43$ isotones, total Routhian surface (TRS) calculations based on a deformed Woods-Saxon cranking model [22] predict that at low energies, before the backbending, this is a moderately deformed band, triaxial or oblate but γ soft, with (β_2, γ) values such as $(0.30, -30°)$ in ^{83}Zr [17], $(0.23, -50°)$ in ^{81}Sr [15], $(0.23, -55°)$ in ^{79}Kr [14], and $(0.22, -50°$ in ^{77}Se) [12]. After the alignment, the band becomes less deformed and nearly prolate or triaxial: $\beta_2 \approx 0.23$. The value at which the kinematic moment of inertia almost saturates after the alignment is about 24, 26, 28, and 29 $\hbar^2$ MeV^{-1} in ^{79}Kr, ^{81}Sr, ^{83}Zr, and ^{85}Mo, respectively; these values are roughly proportional to $A^{5/3}$, suggesting that after the alignment ^{85}Mo has a deformation similar to that of the other isotones.

The negative-parity band is based on the [303]5/2 Nilsson state. In ^{83}Zr it is suggested that it may be admixed with the $K = 1/2$ and 3/2 Nilsson bands [17]. Before the backbending, in all the isotones it is generally calculated as a γ-soft or prolate band, with $\beta_2 \approx 0.26$, while after the backbending it slightly decreases in deformation ($\beta_2 \approx 0.22$) and becomes triaxial [12,14–17].

More detailed considerations concerning the structure of the observed bands are given below.

V. CALCULATIONS FOR ^{85}Mo WITH THE PROJECTED SHELL MODEL

A. Theory

In this section the projected shell model (PSM) is briefly introduced. A more detailed description of the model can be found in the review article of Hara and Sun [23]. The PSM computer code that is used for the present calculation is also accessible [24].

The PSM follows closely the shell model philosophy, and is a spherical shell model truncated in a deformed (Nilsson-type) BCS single-particle basis. More precisely, the truncation is first achieved within the quasiparticle basis with respect to the deformed BCS vacuum $|\phi\rangle$; then rotational symmetry that is violated in the deformed mean-field basis is restored by standard projection technique [25] to form a spherical basis in the laboratory frame; finally the shell model Hamiltonian is diagonalized in the projected basis. The shell model truncation obtained in this way is very efficient. In fact, structure calculation for intermediate and heavy mass regions, which is unfeasible for the conventional shell model due to dimensionality and the related problems, can be efficiently performed by the PSM.

The ansatz for the angular momentum projected wave function is given by

$$|\sigma, IM\rangle = \sum_{\kappa} f_{\kappa}^{\sigma} \hat{P}^{I}_{MK_{\kappa}} |\varphi_{\kappa}\rangle, \tag{1}$$

where the index σ labels the states with the same angular momentum and κ the basis states. $\hat{P}^{I}_{MK}$ is the angular momentum projector [25] which projects good angular momentum from an intrinsic state $|\varphi_{\kappa}\rangle$. In this way, angular momentum conservation, which is violated in the deformed mean-field calculation, is restored.

The basis states $|\varphi_{\kappa}\rangle$ have a good K quantum number, since we start from an axially symmetric potential. In the present calculation the states $|\varphi_{\kappa}>$ are spanned by the following set:

$$\{\alpha^{\dagger}_{n_i}|\phi\rangle, \quad \alpha^{\dagger}_{n_i}\alpha^{\dagger}_{p_j}\alpha^{\dagger}_{p_k}|\phi\rangle\} \tag{2}$$

with $|\phi\rangle$ the quasiparticle (qp) vacuum determined by the Nilsson + BCS calculations. α_m ($\alpha^{\dagger}_m$) are the annihilator (creator) qp operators on this vacuum. The index n_i (p_i) runs over selected neutron (proton) states. The index κ in Eq. (1) runs over the states of Eq. (2). Hereby the standard Nilsson scheme [26] is used for the deformed single-particle calculation. The configuration space includes three major shells, $N = 2$, 3, and 4, for both neutrons and protons.

The weights f^{σ}_{κ} in Eq. (1) are determined by diagonalization of the Hamiltonian $\hat{H}$ in the space spanned by the states of Eq. (2). This leads to the eigenvalue equation (for a given spin I)

$$\sum_{\kappa'} (H_{\kappa\kappa'} - E_{\sigma} N_{\kappa\kappa'}) f^{\sigma}_{\kappa'} = 0, \tag{3}$$

and the Hamiltonian and norm overlaps are given by

$$H_{\kappa\kappa'} = \langle\varphi_{\kappa}|\hat{H}\hat{P}^{I}_{K_{\kappa}K'_{\kappa'}}|\varphi_{\kappa'}\rangle,$$

$$N_{\kappa\kappa'} = \langle\varphi_{\kappa}|\hat{P}^{I}_{K_{\kappa}K'_{\kappa'}}|\varphi_{\kappa'}\rangle. \tag{4}$$

The explicit form of the Hamiltonian is given below.

For a given intrinsic state of Eq. (2), angular momentum projection to different I's generates the rotational band associated with this state. $\hat{P}^{I}_{MK}\alpha^{\dagger}_{n_K}|\phi\rangle$, for example, represents one 1-qp K band in an odd-neutron nucleus. 3-qp bands are built upon a 1-qp neutron band plus a pair of quasiprotons. The energies of the states in the band associated with the intrinsic state $|\varphi_{\kappa}\rangle$ are given by

$$E_{\kappa}(I) = \frac{\langle\varphi_{\kappa}|\hat{H}\hat{P}^{I}_{KK}|\varphi_{\kappa}\rangle}{\langle\varphi_{\kappa}|\hat{P}^{I}_{KK}|\varphi_{\kappa}\rangle} = \frac{H_{\kappa\kappa}}{N_{\kappa\kappa}}. \tag{5}$$

A diagram in which the rotational energies of various bands are plotted against the spin I is referred to [23] as a band diagram.

The Hamiltonian employed in the PSM is [23]

$$\hat{H}=\hat{H}_0-\frac{1}{2}\chi\sum_{\mu}\hat{Q}^{\dagger}_{\mu}\hat{Q}_{\mu}-G_M\hat{P}^{\dagger}\hat{P}-G_Q\sum_{\mu}\hat{P}^{\dagger}_{\mu}\hat{P}_{\mu}, \quad (6)$$

where $\hat{H}_0$ is the spherical single-particle shell-model Hamiltonian and the other terms are quadrupole-quadrupole, monopole-pairing, and quadrupole-pairing interactions, respectively. The strength of the quadrupole-quadrupole force χ is adjusted in such a way that has a self-consistent relation with the employed quadrupole deformation ϵ_2. The monopole-pairing force constants G_M used in the calculations are

$$G^n_M=\left[20.25-16.20\frac{N-Z}{A}\right]A^{-1},$$

$$G^p_M=20.25A^{-1}. \quad (7)$$

These monopole-pairing forces are the same as used in previous PSM calculations for the same mass region [27]. Finally, the strength parameter G_Q for the quadrupole pairing was simply taken to be proportional to G_M. For the present calculation a value of 0.16 was chosen, which is consistent with the value used in the same and the other mass regions [23,27].

B. Results and discussion

The positive-parity band built on the [422]5/2 orbital is interpreted in the previous discussions as having a lower deformation with a triaxial or oblate shape, as also seen for the lighter isotones. Thus, in our calculation, we assume an oblate deformation with $\epsilon_2=-0.24$ for the positive-parity band, and a prolate deformation with $\epsilon_2=0.27$ for the negative parity band.

The PSM result for ^{85}Mo is compared with data in Fig. 6. The PSM calculation reproduces nicely the observed $9/2^+$ band. In particular, the sharpness of the backbending is obtained at the correct rotational frequency. This agreement will allow us to extract physical information as to why and how the backbending occurs, which will be discussed below. The result for the two negative-parity bands is not as impressive as for the positive parity band; the calculated moments of inertia are undervalued and the backbending is too sharp (although there are no sufficient experimental data to disprove this prediction). We may get a better fit if we adjust the interactions (for example, we can decrease the pairing force in order to increase the moments of inertia), but we have chosen not to do so since the basic physics can already be described.

Band diagrams are given in Figs. 7 and 8. In these plots, the various bands presented by curves are calculated according to Eq. (5). The final results, obtained as the lowest state for each spin after band mixing, i.e., after solving the eigenvalue [Eq. (3)], are presented by dots. Not all bands involved in the calculation are plotted. We have selected only those that are important for discussion.

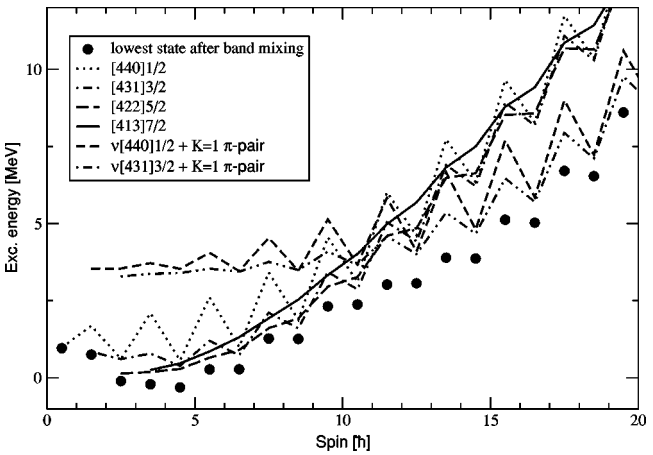

FIG. 7. Band diagram for the positive-parity states of ^{85}Mo. The various bands, as calculated with Eq. (5) are shown by lines, while the lowest states of each spin, obtained after band mixing, Eq. (3), are represented by the black circles.

For the positive-parity case, Fig. 7, one can see four bands starting at energies between 0 and 1 MeV. These are neutron 1-qp bands based on the intrinsic single particles [440]1/2, [431]3/2, [422]5/2, and [413]7/2, respectively. For this nucleus with the neutron Fermi level close to [422]5/2, one expects the band based on [422]5/2 to occur as the lowest band at low spins. Therefore, one can roughly say that the observed positive-parity band is of the [422]5/2 structure since it has its main component from this intrinsic state. However, soon at spin $I=9/2$, the [422]5/2 state is strongly mixed by the other two zigzag bands based on [440]1/2 and [431]3/2. The mixing is so strong that the mixed band carries much character of the low-K band, not that of the [422]5/2 state. The last 1-qp band, the one based on the [413]7/2 configuration, goes up quickly as spin increases, and therefore, does not have much contribution to the mixed states.

There are two interesting observations. First, due to the strong mixing with the [440]1/2 and [431]3/2 configurations at spin $I=9/2$, the mixed state is pushed down so much that

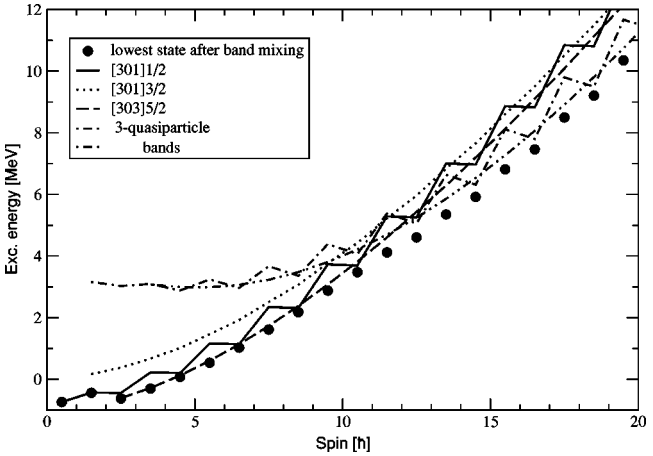

FIG. 8. Same as Fig. 7, but for the negative-parity states.

it becomes lower in energy than the other lower-spin members in this band. This explains why the observed bandhead of the positive-parity band has spin 9/2 although the band has the [422]5/2 structure and should normally have $I=5/2$ as the bandhead. Second, although the positive-parity band is believed to be of the [422]5/2 configuration, it shows a strong decoupling behavior as it is mixed with the [440]1/2 and [431]3/2 configurations. As a consequence, one branch of signature is pushed down and the other up. The states of the unfavored signature are predicted close in energy to those of the favored ones, forming close doublets 7/2-9/2, 11/2-13/2, etc., as observed in the lighter isotones.

In Fig. 7, two bands starting between 3 and 4 MeV cross the 1-qp bands at spin $I=21/2-25/2$. These are 3-qp bands based on intrinsic states of a neutron 1-qp band plus a pair of protons. The most favorite proton pair is built by the intrinsic single particles [422]5/2 and [413]7/2, coupled to $K=1$. Thus, the 3-qp band starting at $I=3/2$ comes from the neutron 1-qp [440]1/2 band plus the $K=1$ proton pair, and the 3-qp band starting at $I=5/2$ comes from the neutron 1-qp [431]3/2 band plus the same $K=1$ proton pair. The observed sharp backbending shown in Fig. 6 can be interpreted as a direct cause of the band crossing discussed above.

In Fig. 8, the band diagram for the negative parity case is displayed. For neutron 1-qp bands, we show three bands based on the intrinsic single particles [301]1/2, [301]3/2, and [303]5/2. Since the neutron Fermi level is close to the negative-parity orbital [303]5/2, the 1-qp band based on this configuration appears to be the lowest. The band based on [301]1/2 lies nearby and shows zigzag behavior. However, in contrast to the positive-parity case, mixing between these two bands appears to be small. Therefore, the [303]5/2 band receives little influence from the mixing, and remains mainly with its smooth behavior. Experimentally, both branches in signature have been observed. The third 1-qp band based on [301]3/2 lies higher in energy, and thus never comes into the yrast region. Therefore, it is of little importance for our discussion.

The observed data stop just around the spin value where the PSM calculation predicts a band crossing. In Fig. 2, one sees that two 3-qp bands starting around 3 MeV cross the 1-qp bands at about spin $I=23/2$.

VI. CONCLUSIONS

In conclusion, we have determined for the first time excited states in the $N=Z+1$ nucleus ^{85}Mo. Two rotational band structures have been observed, which continue smoothly the evolution observed in the lighter $N=43$ isotones and consequently have been assigned as a decoupled $g_{9/2}$ positive-parity band, and a strongly coupled $K=5/2$ negative-parity band, respectively. The similarity of these two band structures along the $N=43$ isotonic chain suggests that in both these bands ^{85}Mo is rather similar to its lighter isotones. Calculations performed with the projected shell model describe reasonably well the behavior with spin of these bands, and give insight into their structure.

Further experimental information on this nucleus would be valuable. Thus, it would be of very much interest to observe experimentally the $\alpha=-1/2$ member of the positive-parity band as well. The signature splitting of this band has a very interesting systematic in the region of the first two band crossings [28] and, once determined also for ^{85}Mo at least up to energies after the first alignment, would give quite useful information concerning the neutron-proton interaction.

ACKNOWLEDGMENTS

This work was partly supported by a research contract with the Romanian Ministry of Education and Research, within the CERES programme. Th.K. and B.Q. acknowledge the EC support under the TMR Contract ERBFMRX-CT97-0123. We thank R. Isocrate for making possible the use of the *n*-Ring detector system.

[1] N. Mărginean, C. Rossi Alvarez, D. Bucurescu, C. A. Ur, A. Gadea, S. Lunardi, D. Bazzacco, G. de Angelis, M. Axiotis, M. De Poli, E. Farnea, M. Ionescu-Bujor, A. Iordăchescu, S. M. Lenzi, Th. Kröll, T. Martinez, R. Menegazzo, D. R. Napoli, G. Nardelli, P. Pavan, B. Quintana, and P. Spolaore, Phys. Rev. C **63**, 031 303(R) (2001).

[2] D. Rudolph, F. Cristancho, C. J Gross, A. Jungclaus, K. P. Lieb, M. A. Bentley, W. Gelletly, J. Simpson, H. Grawe, J. Heese, K.-H. Maier, J. Eberth, S. Skoda, J. L. Durell, B. J. Varley, D. J. Blumenthal, C. J. Lister, and S. Rastikerdar, J. Phys. G **17**, L113 (1991).

[3] W. X. Huang, R. C. Ma, S. W. Xu, X. J. Xu, J. S. Guo, X. F. Sun, Y. X. Xie, Z. K. Li, Y. X. Ge, Y. Y. Wang, C. F. Wang, T. M. Zheng, G. M. Jin, and Y. X. Luo, Phys. Rev. C **59**, 2402 (1999).

[4] D. Bucurescu, C. Rossi Alvarez, C. A. Ur, N. Mărginean, P. Spolaore, D. Bazzacco, S. Lunardi, D. R. Napoli, M. Ionescu-Bujor, A. Iordăchescu, C. M. Petrache, G. de Angelis, A. Gadea, D. Foltescu, F. Brandolini, G. Falconi, E. Farnea, S. M. Lenzi, N. H. Medina, Zs. Podolyak, M. De Poli, M. N. Rao, and R. Venturelli, Phys. Rev. C **56**, 2497 (1997).

[5] C. J. Lister, P. J. Ennis, A. A. Chishti, B. J. Varley, W. Gelletly, H. G. Price, and A. N. James, Phys. Rev. C **42**, R1191 (1990).

[6] M. Campbell, A. A. Chishti, W. Gelletly, L. Goettig, R. Moscrop, B. J. Varley, A. N. James, T. Morrison, H. G. Price, J. Simpson, K. Connel, and O. Skeppstedt, Phys. Rev. Lett. **59**, 1270 (1987).

[7] S. D. Paul, C. Baktash, W. Satula, C. J. Gross, I. Birriel, R. M. Clark, R. A. Cunningham, M. Devlin, P. Fallon, A. Galindo-Urribari, T. Ginter, D. R. LaFosse, J. Kay, F. Lerma, I. Y. Lee, C. Leyland, A. O. Macchiavelli, B. D. MacDonald, S. J. Metcalfe, A. Piechaczek, D. C. Radford, W. Reviol, L. L. Riedinger, D. Rudolph, K. Rykaczewski, D. G. Sarantites, J. X. Saladin, D. Shapira, G. N. Sylvan, S. L. Tabor, K. S. Toth, W. Weintraub, D. F. Winchell, V. Q. Wood, R. Wyss, and C. H. Yu, Phys. Rev. C **58**, R3037 (1998).

[8] D. Bazzacco, Proceedings of the International Conference on Nuclear Structure at High Angular Momentum, Ottawa, 1992

[Report No. AECL 10613], Vol. II, p. 376.
[9] C. Rossi Alvarez *et al.* (unpublished).
[10] E. Farnea *et al.*, Nucl. Instrum. Methods Phys. Res. A **400**, 87 (1997).
[11] N. Mărginean, D. Bucurescu, C. A. Ur, D. Bazzacco, S. M. Lenzi, S. Lunardi, C. Rossi Alvarez, M. Ionescu-Bujor, A. Iordăchescu, G. de Angelis, M. De Poli, E. Farnea, A. Gadea, D. R. Napoli, P. Spolaore, and A. Buscemi, Eur. Phys. J. A **4**, 311 (1999).
[12] G. D. Johns, J. Döring, R. A. Kaye, G. N. Sylvan, and S. L. Tabor, Phys. Rev. C **55**, 660 (1997).
[13] G. D. Johns, J. Döring, J. W. Holcomb, T. D. Johnson, M. A. Riley, G. N. Sylvan, P. C. Womble, V. A. Wood, and S. L. Tabor, Phys. Rev. C **50**, 2786 (1994).
[14] R. Schwengner, J. Döring, L. Funke, G. Winter, A. Johnson, and W. Nazarewicz, Nucl. Phys. **A509**, 550 (1990).
[15] E. F. Moore, P. D. Kottle, C. J. Gross, D. M. Headly, U. J. Hütmeier, S. L. Tabor, and W. Nazarewicz, Phys. Rev. C **38**, 696 (1988).
[16] D. H. Smalley, R. Chapman, P. J. Dagnall, C. Finck, B. Haas, M. J. Leday, J. C. Lisle, D. Prevost, H. Savajols, and A. G. Smith, Nucl. Phys. **A611**, 96 (1996).
[17] V. J. Hüttmeier, C. J. Gross, D. M. Headly, E. F. Moore, S. L. Tabor, T. M. Cormier, P. M. Stwertka, and W. Nazarewicz, Phys. Rev. C **37**, 118 (1988).
[18] D. Rudolph, C. J. Gross, K. P. Lieb, W. Gelletly, M. A. Bentley, H. G. Price, J. Simpson, B. J. Varley, J. L. Durell, O. Skeppstedt, and S. Rastikerdar, Z. Phys. **338**, 139 (1991).
[19] K. Jonsson, B. Cederwall, A. Johnson, R. Wyss, T. Back, J. Cederkall, M. Devlin, J. Elson, D. R. LaFosse, F. Lerma, D. G. Sarantites, R. M. Clark, I. Y. Lee, A. O. Macchiavelli, and R. W. Macleod, Nucl. Phys. **A645**, 47 (1999).
[20] H. G. Price, C. J. Lister, B. J. Varley, W. Gelletly, and J. W. Olness, Phys. Rev. Lett. **51**, 1842 (1983).
[21] D. Rudolph, C. J. Gross, Y. A. Akovali, C. Baktash, J. Döring, F. E. Durham, P.-F. Hua, G. D. Johns, M. Korolija, D. R. LaFosse, I. Y. Lee, A. O. Macchiavelli, W. Rathbun, D. G. Sarantites, D. W. Stracener, S. L. Tabor, A. V. Afanasjev, and I. Ragnarsson, Phys. Rev. C **54**, 117 (1996).
[22] W. Nazarewicz, J. Dudek, R. Bengtsson, T. Bengtsson, and I. Ragnarsson, Nucl. Phys. **A435**, 397 (1985).
[23] K. Hara and Y. Sun, Int. J. Mod. Phys. E **4**, 637 (1995).
[24] Y. Sun and K. Hara, Comput. Phys. Commun. **104**, 245 (1997).
[25] P. Ring and P. Schuck, *The Nuclear Many-Body Problem* (Springer Verlag, New York, 1980).
[26] T. Bengtsson and I. Ragnarsson, Nucl. Phys. **A436**, 14 (1985).
[27] R. Palit, J. A. Sheikh, Y. Sun, and H. C. Jain, Nucl. Phys. **A686**, 141 (2001).
[28] S. L. Tabor, J. Döring, and I. Ragnarsson, Proceedings of the International Workshop ''Selected Topics on N=Z Nuclei,'' PINGST 2000, Lund, 2000, p. 58.